Proceedings of the ASME 2024
Internal Combustion Engine Division ICE Forward Conference
ICEF2024
October 20–23, 2024, San Antonio, TX

ICEF2024-142853

COMPARISON OF A FULL-SCALE AND A 1:10 SCALE LOW-SPEED TWO-STROKE MARINE ENGINE USING COMPUTATIONAL FLUID DYNAMICS

Flavio Dal Forno Chuahy*, Charles E.A. Finney, Brian C. Kaul, Michael D. Kass

Oak Ridge National Laboratory, Oak Ridge, Tennessee USA

ABSTRACT

International marine shipping is a growing component of international trade; a vast majority of all the world's goods are being transported on large ocean-going vessels. The International Maritime Organization (IMO) introduced the Energy Efficiency Design Index (EEDI) in 2013, a regulatory framework of associated metrics for reducing emissions of CO_2 per tonne-mile from shipping by approximately 10% each decade. Therefore, decarbonizing the maritime sector requires the development of new fuel sources. Because of the extremely large physical size of the internal combustion engines present in shipping vessels, experimental iterative development of the engine and fuel system is cost-prohibitive. Thus, the ability to perform combustion system development in a scaled platform that can be more easily operated and modeled computationally is of interest. To that end, scaling relationships are needed to translate the results from a smaller engine to a larger counterpart. Scaling studies to date have been restricted to low scaling ratios, four-stroke light-duty engines, and under-resolved computational fluid dynamic simulations that likely do not accurately capture the physics of scaling. In this work, computational models of a 1:10 scale and a full-scale two-stroke crosshead low-speed marine engine were created and validated against experiments obtained in a real 1:10 scale engine installed at Oak Ridge National Laboratory (ORNL). Due to the large size of the full-scale engine, the model required large high-performance computing resources to be evaluated. The availability of high-performance computing resources at the Department of Energy's Leadership Computing Facilities is an enabler of the current work. The results of the small- and large-scale engine simulations were compared to analyze the effectiveness of the appropriate scaling laws under these extreme scaling ratio conditions.

Keywords: marine, two-stroke, combustion, scaling, diesel

1. INTRODUCTION

Global marine fuel consumption amounts to over 105 billion gallons of fuel each year and is expected to double by 2030 because of the expansion in global trade [1]. This represents several times the annual consumption of cars and trucks in the United States. The international maritime organization (IMO) introduced the Energy Efficiency Design Index (EEDI) in 2013, a regulatory framework of associated metrics for reducing emissions of CO_2 per tonne-mile from shipping by approximately 10% each decade. IMO has also implemented several fuel quality and criteria pollutant standards. Heavy fuel oil (HFO) represents 76%, marine diesel oil (MDO) 21%, and liquefied natural gas 3% of annual marine fuel consumption, as of 2012 [2]. The required fuel changes due to new regulations will involve the use of much costlier distillate fuels such as MDO. Additionally, Smith et al. [3] estimate that CO_2 emissions derived from marine shipping may increase by 50–250% by 2050, depending on economic growth. Accordingly, adoption of lower-carbon fuels in the marine sector has both regulatory and economic motivators, which led to recent responses from the shipping industry. Therefore, to fulfill the promise of a net-zero marine shipping sector by 2050, reduced or net-zero carbon fuels, de-sulfurization, and black carbon reductions will be needed.

Decarbonizing the maritime sector, then, requires the development of new fuel sources. Due to the extremely large physical size of the internal combustion engines present in shipping vessels, experimental iterative development of the engine–fuel system is cost-prohibitive. Therefore, the ability to perform combustion system development on a scaled platform that can be more easily operated and modeled computationally is of interest. To that end, scaling relationships are needed that can directly translate results from a smaller engine to its larger counterparts. Engine size scaling has been an area of active research for over 100 years [4]. However, because of the limited experimental

*Corresponding author: dalfornochuf@ornl.gov

validation data and computational resources, research on scaling has been mostly restricted to small-bore engines representative of light-duty engines and are not representative of the large-scale two-stroke marine engines. Ideally, results from a scaled-down platform can be scaled-up with simple relationships to achieve the same brake thermal efficiency and power-specific emissions for any arbitrary design. Achieving perfect scaling is a challenging goal—particularly for extremely large engines, such as the 1000 mm bore marine shipping engines. This is because inertial forces and material constraints limit the speeds at which the engine can operate, thereby limiting scaling of metrics such as friction, heat transfer, and turbulent timescales, which depend on the mean piston speed (MPS). Large bore engines also have a lower surface-to-volume ratio than small bore light-duty engines, which directly affects the heat transfer characteristics of the engine.

A substantial amount of work has been done to develop scaling laws for conventional diesel combustion, the combustion mode relevant to marine engines. The idea of engine scaling was proposed by Bergin et al. [5]. In their simple scaling model, all geometric parameters were scaled to the ratio between the engine bore sizes, and the injection parameters were scaled to achieve scaled spray penetration length. Extensions of that work by Stager et al. [6] proposed an extended scaling model that introduced provisions to account for lift-off length scaling. This extended scaling model was explored by Shi et al. [7] using computational fluid dynamics (CFD) simulations and found acceptable predictive capability. Similarly, Lee et al. [8] studied the sensitivity of several scaling parameters on the outputs using CFD. Their objective was to explore potential limitations, such as physical constraints, on the ability of scaled engines to reproduce the results of larger ones. They found that the extended scaling very accurately predicted performance and emission trends. However, they suggested that a scaling by which the engine speed is held constant would be the most appropriate, which by consequence also keeps the injection duration constant. Tess et al. [9] explored that same speed scaling and showed it to be the best scaling method for their conventional diesel combustion conditions.

Large-scale marine engines have fundamentally different architectures than typical four-stroke engines. Figure 1 shows a comparison of a typical four-stroke engine architecture with a section of the piston profile and that of a two-stroke low-speed marine engine. Figure 1 also shows a comparison of piston sizes to scale. It is clear that there is a substantial size difference between the engines used in past scaling studies and two-stroke engines of a size relevant to ocean-going vessels. Architecturally, these engines are also extremely different. A typical heavy-duty four-stroke engine has two intake and two exhaust valves, a centrally mounted injector with an axi-symmetric spray pattern, and a re-entrant style piston bowl. In contrast, a two-stroke marine engine has a single exhaust valve and intake ports placed around the cylinder liner, multiple tangentially mounted injectors with an asymmetric nozzle pattern, and a shallow bowl profile. These differences in architecture and size result in combustion timescales that are completely different. The mean piston speed of both engines is similar, but the rotational speed of large marine engines is significantly lower, leading to a much longer wall-clock time available for fuel mixing and combustion. Therefore, given the extreme size differences, architectural differences, and timescale differences, scaling relationships developed thus far, in which the engine speed is matched, are not relevant and cannot be used. Additionally, it is plausible that new metrics should be considered when attempting to scale engine results from large marine engines.

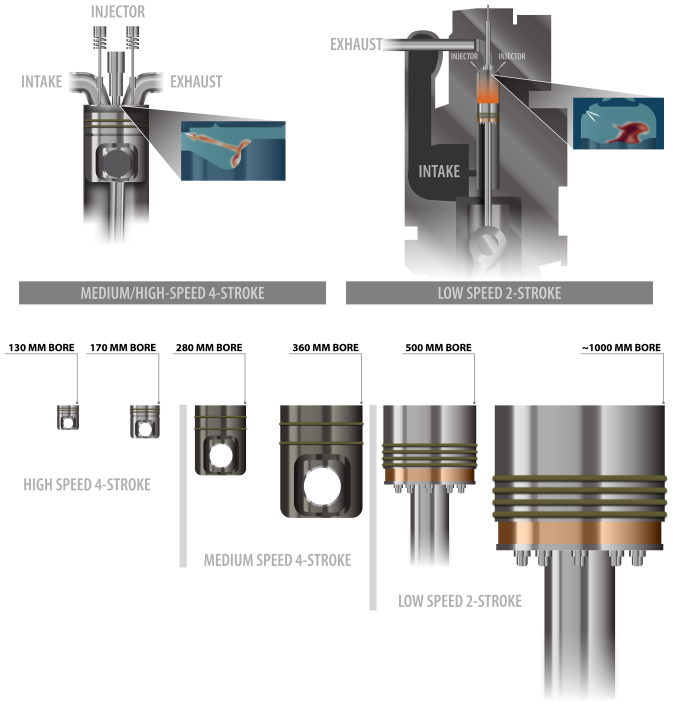

FIGURE 1: Comparison of typical four-stroke diesel engine and two-stroke low-speed marine engines, as well as a comparison of piston size between a heavy-duty engine and an ocean-going marine two-stroke engine. Reproduced from [10].

Researchers have recently published several articles on marine engine scaling efforts [11–15]. Most recent and past studies have relied on coarse, low-fidelity computational meshes to reduce computing time when modeling large geometries. This approach reduces the accuracy of the predictions and the validity of the conclusions. Likewise, simulations have been limited to maximum bore sizes of ~500 mm, which do not represent the full range of low-speed marine engines (with bore sizes up to ~1000 mm). Zhou et al. [12] attempted to show the impact of engine size when increasing the bore size from 340 to 520 mm. However, computational cell sizes increased as the bore size increased to reduce the computational burden, and cell sizes were substantially larger than recommended to resolve the turbulence length scales of interest. Furthermore, simulations of large engine scaling have typically been restricted to the closed cycle portion of the engine cycle—that is, the effects of flow field changes during the intake process are not captured. Zhou et al. [15] substantially expanded their computational work on marine engine scaling by applying three different scaling methods, a simple scaling, which

TABLE 1: 1:10 Scaled Engine Configuration

Bore	[mm]	108
Stroke	[mm]	432
Connecting Rod Length	[mm]	750
Geometric Compression Ratio	[–]	13
Number of Injectors	[–]	2
Number of Nozzles per Injector	[–]	3

they refer to as "P Law"; Stager's extended scaling, referred to as "L Law"; and the same speed scaling, referred to as "S Law". Simple scaling, or the "P Law", was the only scaling law that allowed scaling up to 1020 mm bore size. "L Law" and "S Law" scaling were limited by the MPS, with the same engine speed law being the most restricted. Therefore, for large similarity ratios (e.g., > 5.0), scaling is restricted to the "P Law". It is important to note that the "P Law" showed the worst scaling for emissions metrics like NOx and soot; thus, a trade-off is clear between scaling accuracy and similarity ratios. Like their previous work, however, the computational cell size was scaled by the similarity ratio to reduce computational cost. The assumption that turbulent length scales scale with the similarity ratio has not been demonstrated. Given that the smallest turbulent length scales (i.e., the Kolmogorov length scale) are proportional to the fluid's kinematic viscosity and turbulent dissipation rate, it is more likely that the minimum cell size for accurate resolution stays the same between a small and large engine.

Studies to date have been restricted to low scaling ratios (a maximum of 3× in Zhou et al.'s work [15]), four-stroke light-duty engines, and under-resolved CFD simulations performed in close-cycle simulations. Consequently, there is a need to computationally explore scaling at much larger similarity ratios and with the appropriate computational resolution, such that these scaling laws can be used to guide future marine engine design. In this work, a computational model of a 1:10 scale and a full-scale two-stroke crosshead low-speed marine engine were created with the appropriate computational resolution. The scaled model was then validated against experiments obtained in the scaled engine, and the effectiveness of simple scaling laws under these extreme conditions in scaling heat release rates, mixing, and emissions was analyzed.

2. METHODS

Table 1 shows the baseline engine configuration used for validation and modeling. The engine is a one-of-a-kind, custom-built, single-cylinder, uniflow scavenged, two-stroke crosshead marine diesel engine. The engine was designed to be a 1:10 scale version of a full-scale marine engine. The engine has a 108 mm bore and a 432 mm stroke, with a geometric compression ratio of 13:1. The engine has two tangentially mounted injectors with three nozzles per injector in an asymmetric pattern. More details on the construction and design of the engine can be found in Kaul et al. [16].

A fuel surrogate was developed for diesel fuel and is shown in Table 2. The mechanism used was reduced from a detailed mechanism developed by the CRECK modeling group [17, 18].

TABLE 2: Chemical surrogate composition for conventional diesel

Chemical Species	Component [% Mole]
n-Decane	59.5
Toluene	20
iso-Octane	10
methyl-Cyclohexane	10.5

TABLE 3: Summary of modeling setup for engine simulations

CFD Software	CONVERGE 3.0.15
Fuel Injection	Blob
Droplet Break-up	KH–RT
Droplet Collision	NTC
Droplet Drag	Dynamic
Droplet Evaporation	Frossling Correlation
Combustion	SAGE with adaptive zoning
Turbulence	RNG k–ϵ
Base mesh size in cylinder	4 mm
Adaptive mesh refinement (AMR)	0.25 mm (validation)
Cell size based on temp. and velocity	0.5 mm (scaling)
NOx emissions	Direct Chemistry

The mechanism was chosen because of the availability of relevant alkanes, cycloalkanes, and aromatic species for diesel combustion. More details on the mechanism development can be found on Chuahy et al. [19].

Table 3 shows a summary of the 3D CFD setup used for the simulations. CFD simulations were performed using CONVERGE 3.0.15. Grid parameters were defined based on the experimental validation and defined base mesh size and adaptive mesh refinement settings. Multi-component evaporation was considered. Combustion was solved through direct chemistry integration using a well-stirred reactor assumption coupled with an adaptive zoning scheme. The fuel spray was simulated with the typical sub-models available in CONVERGE and are summarized in Table 3. NOx emissions were simulated through a sub-mechanism for thermal and prompt NOx formation present in the chemical mechanism used. Turbulence was modeled using a conventional Reynolds-averaged Navier–Stokes (RANS) re-normalization group (RNG) k–ϵ approach.

2.1 Model Validation

The model was validated against experimental data taken for the scaled engine summarized on Table 1. The condition chosen for validation is a high-speed/high-load condition with a nominal load of 14 bar indicated mean effective pressure (IMEP). Table 4 summarizes the engine operating condition. The engine was operated at 545 rpm with an intake pressure of 3.07 bar and an intake temperature of 40°C. The total fuel energy was 7383 J per injector per engine cycle, which resulted in a global equivalence ratio (ϕ) of 0.41. Figure 2 shows a comparison of in-cylinder pressure and heat release rate for simulations and experiments. The results show that the model can very accurately capture the ignition delay, the transition from the premixed heat release and the main heat release, and the end of the heat release

process, and they are within experimental variations. Table 5 shows a comparison of the measured NOx emissions in ppm and the results from the model. For the chosen validation condition, mean NOx emissions were 1164 ppm, with a standard deviation of 26 ppm. The simulation predicted NOx emissions of 1191 ppm for the same condition, a good match against measured values.

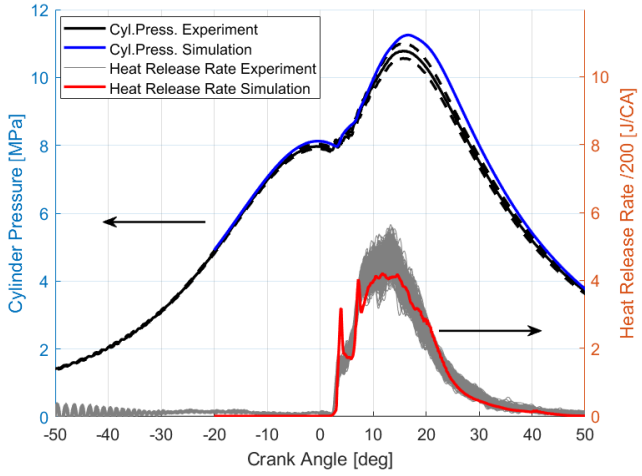

FIGURE 2: Comparison of experimental and simulated in-cylinder pressure and apparent heat release rate for conventional diesel and renewable diesel under the same conditions. Dashed line in experiments represents ±1 standard deviation from the mean. All collected cycles are shown for the heat release rate.

TABLE 4: Summary of operating conditions used for validation and scaling study.

Engine Speed [rpm]	545
Intake Pressure [bar]	3.07
Intake Temperature [K]	40
Injection Duration [°CA]	17.6
Fuel Energy [J/injector/cycle]	7383
Nominal Engine Load [bar]	14
Global Equivalence Ratio [–]	0.41
Exhaust Gas Recirculation [%]	0

TABLE 5: Comparison of NOx emissions between conventional diesel experiments and conventional diesel CFD results

	Experiments	Simulation
NOx [ppm]	1164 ± 26	1191

2.2 Grid Settings and Initialization

To keep the number of total cells in the full-scale engine model under control, settings for the adaptive mesh refinement (AMR) scheme were modified from those used in the validation. The minimum cell size for both models used in the comparison was increased from 0.25 mm, used in the model validation, to 0.5 mm. The results for the 1:10 scale model change with this increase in cell size and the model results are less accurate when compared to experiments. However, there were no significant changes, and the model was still observed to be capable of capturing the experimental heat release fairly accurately. Therefore, this is believed to be an appropriate relaxation of the grid resolution to allow a direct comparison between scaled and full-scale models. Even with this increase in the AMR settings, the number of cells for the full-scale model was extremely high. Figure 3 shows a comparison of the total cell count during the simulations between the scaled and full-scale engine. Whereas the scaled model peaked at approximately 0.7M cells, the full-scale model reached as high as 100M total cells, being then one of the largest internal combustion engine simulations ever performed.

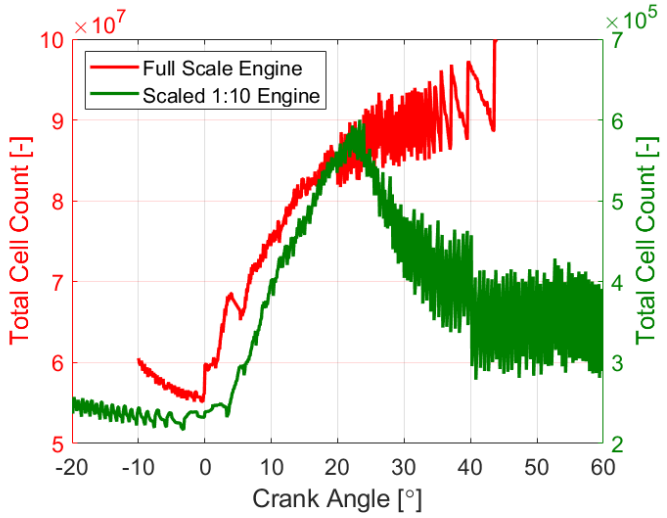

FIGURE 3: Comparison of total cell count during the simulation between scaled and full-scale engines.

The full-scale model was initialized at −10°CA after top dead center of firing (aTDCf) to save computational time during the scavenging and compression processes. The flow field and thermodynamic conditions from the scaled model were mapped onto the full-scale grid to start the simulation with a realistic flow structure. Therefore, these simulations do not take into account the potential differences in scavenging from the full-scale to the scaled engine.

2.3 Scaling Law

As mentioned in the introduction, the large scaling ratios involved in this work and the unprecedented size of the full-scale simulation preclude the use of any scaling relationship that does not involve a matching of the mean piston speed. Use of the "L Law" and "S Law" would result in excessive mean piston speeds for the full-scale engine that are not feasible in practice and would lead to excessive mechanical loads. Therefore, for this work, the simple scaling relationship was used, which maintains a constant mean piston speed of the engines. Table 6 shows a summary of the scaling ratios for all the parameters of interest. In the simple scaling approach, all geometric features are scaled by the scaling ratio L. The volume of the engine, therefore, was scaled by L^3. To maintain the injection pressure and the duration of the injection in crank angle space, the fuel mass was scaled by the same engine

TABLE 6: Scaling ratios for all parameters of interest.

Parameter	Scaling Factor
Bore	L
Stroke	L
Connecting Rod	L
Cylinder Displacement	L^3
Base Cell Size	1
AMR Refinement	1
Injector Nozzle Diameter	L
Injection Duration (Time Space)	L
Injection Duration (Crank Space)	1
Injection Pressure	1
Engine Speed	L^{-1}
Number of Injected Fuel Parcels	L
Fuel Energy	L^3
Intake Pressure	1
Intake Temperature	1

displacement volume ratio. Thermodynamic conditions and grid settings were maintained for each of the simulations. Engine speed was scaled by the inverse of the scaling ratio.

One of the main challenges with these simulations is the spray model. The KH–RT spray model that is typically used to simulate engine diesel sprays and break-up has not been validated for large scales, and scaling studies have not been conducted to determine the behavior of this break-up model under scaling ratios like the one attempted here. Ideally, the number of injected fuel parcels would be scaled with the total fuel mass such that the amount of fuel per injected parcel remained constant. However, this would imply a total of 500M parcels injected per injector; along with parcel break-up during the injection event, the number of parcels would grow several times. With potentially over a billion parcels to be tracked by the model, computing times would become intractable. Beyond computing times, memory requirements for such a large number of tracked parcels would be beyond even the super-computing nodes used for the current simulations. To enable the large-scale simulation being performed, the number of injected parcels was scaled by L and not L^3. Scaling studies of spray behavior with large scaling ratios and validation of the KH–RT break-up model under these extreme conditions must be conducted for improved results in the future.

2.4 High-Performance Computing

Simulations for the large-scale model were performed on the Theta Supercomputer at Argonne National Laboratory. The model was partitioned into 8,191 total cores for an approximate total cell count of 10,000 cells per core.

3. RESULTS AND DISCUSSION

Figure 4 shows the comparison between the in-cylinder pressure and apparent heat release rates (AHRR) for the scaled and full-scale models. The results show that the AHRR and in-cylinder pressure traces were fairly similar between the two models, with some key differences. The full-scale model shows a shorter ignition delay and no premixed heat release spike during the first stage of the heat release. The transition between the first-stage heat release and the main heat release occurred around the same time for both simulations. The overall peak heat release rate was similar for both cases, with the scaled case showing an early spike. The tail end of the heat release was similar for both cases, resulting in similar total combustion durations.

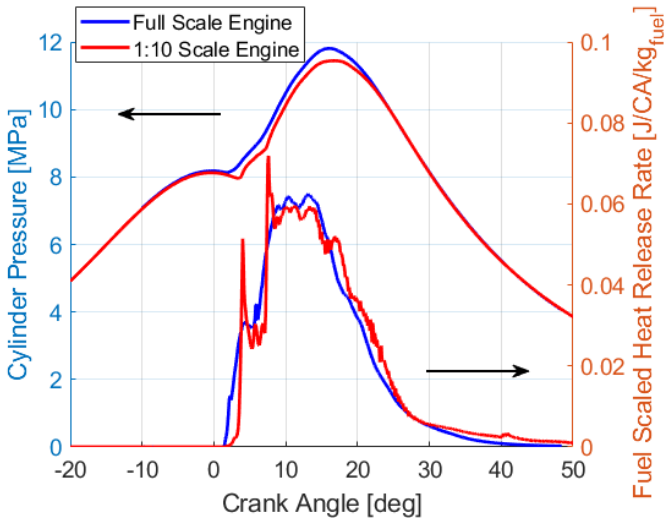

FIGURE 4: Comparison of in-cylinder pressure and apparent heat release rate for scaled and full-scale engines.

The simple scaling relationship seems to have appropriately scaled the AHRR observed in the scaled engine to the full-scale engine. However, more detailed information of the mixing and combustion process need to be compared to determine whether the simple scaling was successful in appropriately scaling emissions and other metrics. Figure 5 shows a comparison of the equivalence ratio distributions as a function of crank angle for the scaled and full-scale engines. The fuel is binned into different ranges of ϕ for comparison. The results show that the ϕ distributions are significantly different, particularly after 10°CA aTDCf. The results show that for the scaled engine the fuel mixture became more stratified, indicating significant differences in fuel break-up, evaporation, and mixing. More fuel was present in rich regions of $1.0 < \phi < 2.0$, and less fuel was present lean regions of $\phi < 0.5$. To take a more detailed look into the mixture preparation during combustion, mass-weighted probability density function (PDF) distributions of the ϕ values can be compared at key points during the combustion process. Figure 6 shows a comparison of the mass-weighted PDF of ϕ for the scaled and full-scale engines at a crank angle of 10% mass fraction burned (CA10), CA50, and CA90. The computational cells were filtered to include only those locations where the local ϕ was higher than 0.5 to enable a focus on the spray and subsequent mixing. The results show that the scaled engine resulted in higher fuel stratification at the start of combustion (CA10), as illustrated by the wider ϕ distribution and higher values of ϕ. For the full-scale engine, mixtures were observed to be more concentrated in the region near a $\phi = 1.0$ (stoichiometry). Halfway through the combustion process (CA50), mixtures were still very different between the two simulations. The scaled engine had a large portion

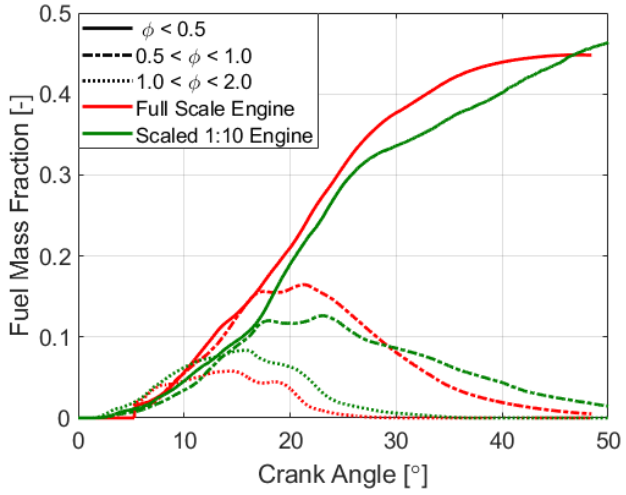

FIGURE 5: Comparison of equivalence distributions as a function of crank angle for scaled and full-scale engines.

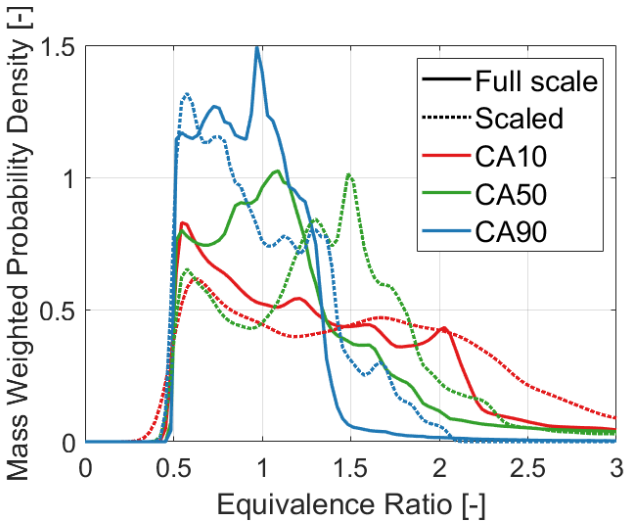

FIGURE 6: Comparison of the probability density distribution of equivalence ratio at CA10, CA50, and CA90 for scaled and full-scale engines.

of the fuel in regions of $\phi > 1.5$, whereas the full-scale engine continued to have a higher portion of the fuel near stoichiometric mixtures. At the end of the combustion process (CA90), the trend continued: the scaled engine shows a more stratified mixture, with a significant portion of the fuel in regions of $\phi > 1.5$. These trends illustrate that there were significant differences in the mixing process between the two cases. This is expected for a simple scaling due to the changes in time-scales. In the full-scale engine, the fuel had a significantly longer wall-clock time for mixing due to the lower engine speed, which drove previous works to conclude a same-speed scaling was the best approach. However, as explained previously, that approach is not feasible for the majority of relevant scaling ratios desired for marine engines.

To enable a visualization of the fuel distribution, Figure 7 shows a top-view comparison of the two simulations at CA10. The spray is represented by an iso-surface of $\phi = 2.0$ colored by temperature, and the combustion process is represented by the yellow iso-surface of T = 2650 K. The ϕ iso-surfaces show that the distribution of fuel immediately after injection was already very distinct between the fuels. The $\phi = 2.0$ iso-surface for the full-scale engine was much larger and wider near the injector nozzle. Although not shown in Figure 6, the near-nozzle region of the full-scale model has much richer fuel–air mixtures—despite the wider ϕ distribution observed for the scaled model. For the scaled model, mixtures no higher than $\phi = 5.0$ were observed. For the full-scale model, mixtures with $\phi > 8.0$ were observed near the nozzle exit at CA10. The different shape of the ϕ iso-surface and the differences in the near-nozzle fuel–air mixtures indicate that there may be significant differences in the behavior of the spray and break-up models between the different sizes. The temperature profiles are also very distinct between the simulations. The scaled simulation shows that the first injection jet was partially ignited. The region at the base of the jet had not ignited at the point shown. The temperature iso-surface shows that the highest temperatures were located near the leading edge of the fuel plume. The second injection can be seen, but at CA10 it had not yet ignited. In contrast, the full-scale simulation shows that the first injection jet seems to have completely ignited, including the base of the jet. The temperature iso-surface enveloped the entire ϕ iso-surface and covered a much wider volume than that observed in the scaled simulation. The first injection ignition appears to have allowed fast ignition of the second injection. These differences led to the differences observed in ignition delay, the faster initial rate of combustion, and the absence of a premixed spike toward the end of the first stage heat release.

Figure 8 shows the PDF of temperature at CA10, CA50, and CA90 and illustrates further the differences in internal thermodynamic conditions between the cases. At CA10, what was observed in Figure 7 is further illustrated. The overall temperature profiles were similar. However, the full-scale engine showed higher temperature regions when T > 2100 K. Spikes in the PDF were observed at temperatures of 600 K to 1000 K, which represent the non-ignited second injection for the scaled engine. The spike was not observed for the full-scale engine due to the second injection being already ignited at CA10. The trend of higher temperatures was observed for CA50 and CA90, with higher peak temperatures and a higher frequency of regions at higher temperatures for the full-scale engine. This is likely the result of the ϕ distributions shown previously, where the full-scale engine resulted in a larger portion of the fuel–air mixture in ratios near stoichiometry. These mixtures had a higher adiabatic flame temperature, which is monotonically reduced above and below a $\phi = 1.0$.

Figure 9 shows the PDFs of NO mass fraction and soot predicted by the Hiroyasu model. The results show that the full-scale simulation resulted in higher emissions of NO. This is a result of the higher temperatures observed for the full-scale model, as the main mechanism for nitrogen oxide formation is thermal in nature. Soot emissions followed the same trend. The Hiroyasu soot models the competition between soot formation and oxidation to predict total soot mass during combustion. The soot formation model uses a simple Arrhenius expression that

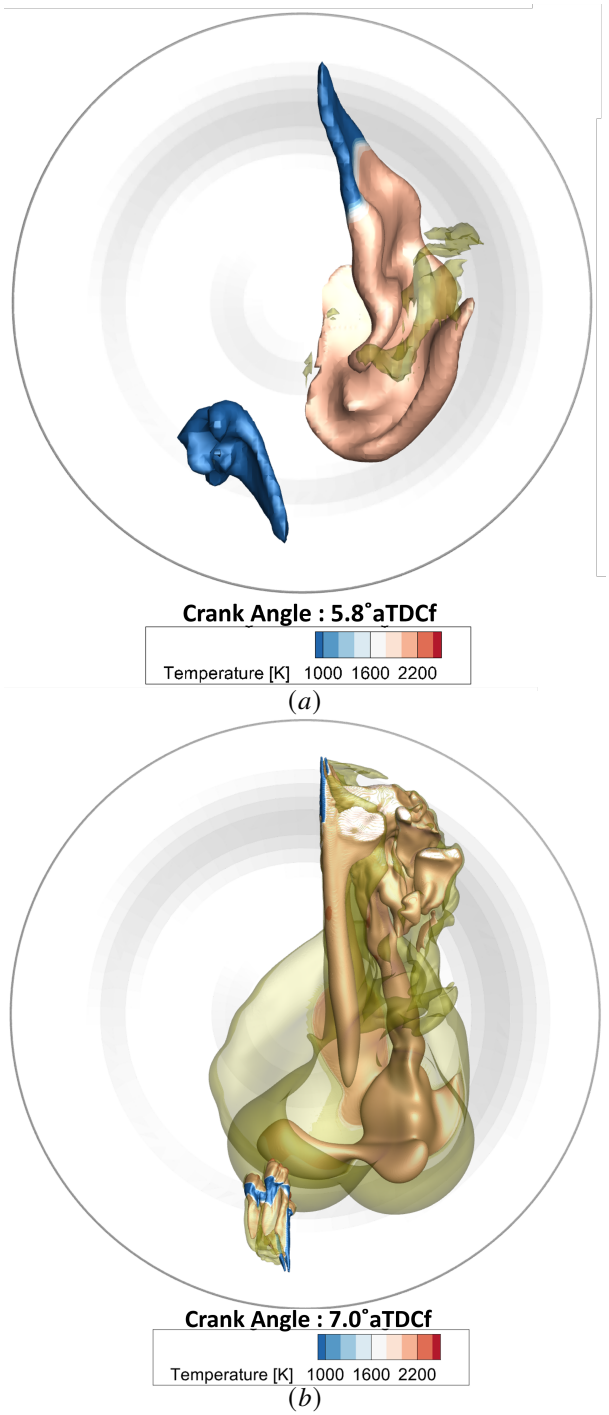

FIGURE 7: Cylinder top view for (a) scaled and (b) full-scale engines. Spray is represented by an iso-surface of $\phi = 2.0$ colored by temperature, and the combustion process is represented by the yellow iso-surface of T = 2650K. Images shown at CA10.

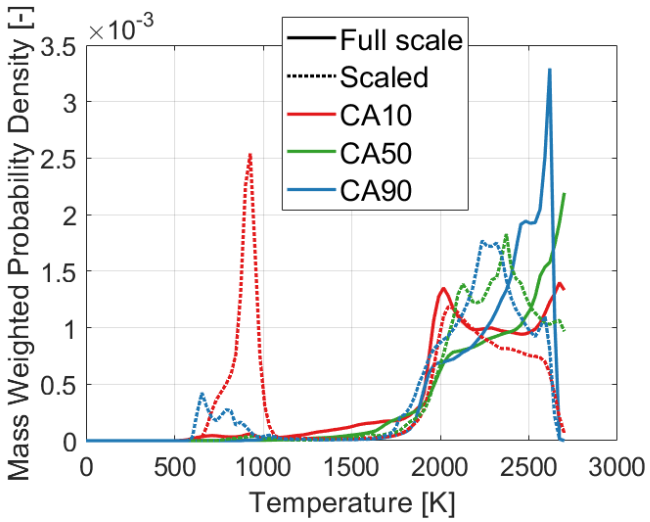

FIGURE 8: Comparison of the probability density distribution of temperature at CA10, CA50, and CA90 for scaled and full-scale engines.

functions as the formation rate of soot, based on the total amount of unburned hydrocarbons available (as inception species) and the local thermodynamic conditions. Therefore, it is clear that the larger peak equivalence ratios and larger amounts of fuel in hotter near-stoichiometric mixtures led to the increase in soot predictions observed.

Analysis of the results shows that the simple scaling relationship closely reproduced the AHRR of the scaled engine with some differences. However, the scaling was not capable of reproducing the fuel spray break-up and mixing of the scaled engine, which resulted in significant differences in ϕ distributions, temperatures, and, therefore, emissions. Differences can likely be traced back to the fact that the simple scaling applied does not scale for the same lift-off length like the "L Law" scaling, nor the same mixing time-scales like the "S Law" provides. Additionally, it is unclear how much of the difference is dictated by the spray model itself, with the higher fuel mass per parcel and its behavior at these large scales. Consequently, new scaling relationships must be developed—or, at a minimum, correlations should be established between scales using this simple scaling—if scaled platforms are to be utilized for full-scale engine combustion system development.

4. CONCLUSION

In this work, a large scale simulation of a marine two-stroke engine was performed using high-performance computing. The results show that due to the large scaling ratios needed to enable experimental development of new marine engine combustion systems, only simple scaling relationships can be used (i.e., a scaling relationship that maintains the engine's mean piston speed). The simple scaling relationship performed relatively well in reproducing the overall heat release rate profile of the scaled engine. However, there were significant discrepancies in the mixing characteristics that resulted in significantly different emissions profiles, with the full-scale engine showing higher NO and soot emissions predictions. Additionally, the spray model used for these

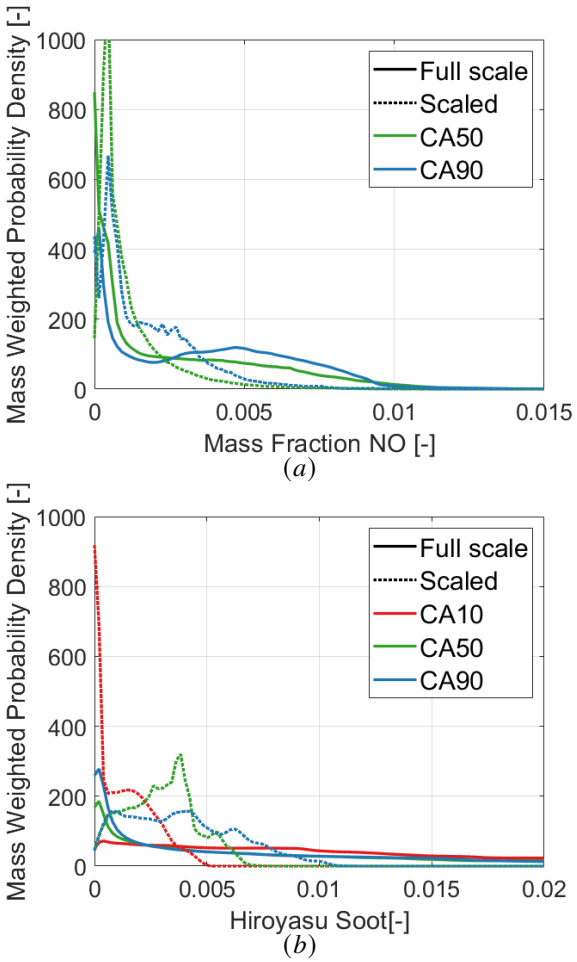

FIGURE 9: Comparison of probability density distribution with respect to (a) NO mass fraction and (b) Hiroyasu soot at CA10, CA50, and CA90 for scaled and full-scale engines.

simulations has not been validated at the large scales relevant to two-stroke marine engines. With potentially large changes in the Weber number for larger injectors, the break-up regime may be significantly different than that for a 1:10 scaled version of the injector.

Future work should focus on (1) establishing appropriate scaling relationships for the fuel injection process through high-fidelity simulations and validating different break-up models that are appropriate for large similarity ratios like the one shown here and (2) characterizing the potential differences in flow field during scavenging between scaled and full-scale engines.

ACKNOWLEDGMENTS

The authors acknowledge funding from the Laboratory Directed Research and Development (LDRD) program at Oak Ridge National Laboratory. This research used resources of the Compute Data Environment for Science (CADES) at Oak Ridge National Laboratory, which is supported by the Office of Science of the US Department of Energy under Contract No. DE-AC05-00OR22725 and from the Theta Supercomputer at Argonne National Laboratory. The authors thank Convergent Science, Inc. for providing licenses to CONVERGE, which enabled this work.

REFERENCES

[1] "Billion Ton Report." Technical report no. Bioenergy Technologies Office. 2016, Accessed 04/11/2024. URL https://www.energy.gov/eere/bioenergy/2016-billion-ton-report.

[2] "Marine Fuel Facts." Technical report no. Concawe. 2017, Accessed 04/11/2024. URL https://www.concawe.eu/wp-content/uploads/2017/01/marine_factsheet_web.pdf.

[3] Smith, Tristan. "Definition of Zero Carbon Energy Sources." Technical report no. Global Maritime Forum. 2019. URL https://www.globalmaritimeforum.org/content/2019/09/Getting-to-Zero-Coalition_Zero-carbon-energy-sources.pdf.

[4] Lanchester, F. W. "The Horse-Power of the Petrol Motor in its Relation to Bore, Stroke and Weight." *Proceedings of the Institution of Automobile Engineers* Vol. 1 No. 2 (1906): pp. 153–220. DOI 10.1243/PIAE_PROC_1906_001_008_02. URL https://doi.org/10.1243/PIAE_PROC_1906_001_008_02, URL https://doi.org/10.1243/PIAE_PROC_1906_001_008_02.

[5] Bergin, Michael J., Hessel, Randy P. and Reitz, Rolf D. "Optimization of a Large Diesel Engine via Spin Spray Combustion." *SAE 2005 World Congress Exhibition*. 2005. SAE International. DOI https://doi.org/10.4271/2005-01-0916. URL https://doi.org/10.4271/2005-01-0916.

[6] Stager, Laine A. and Reitz, Rolf D. "Assessment of Diesel Engine Size-Scaling Relationships." *SAE World Congress Exhibition*. 2007. SAE International. DOI https://doi.org/10.4271/2007-01-0127. URL https://doi.org/10.4271/2007-01-0127.

[7] Shi, Yu and Reitz, Rolf D. "Study of Diesel Engine Size-Scaling Relationships Based on Turbulence and Chemistry Scales." *SAE World Congress Exhibition*. 2008. SAE International. DOI https://doi.org/10.4271/2008-01-0955. URL https://doi.org/10.4271/2008-01-0955.

[8] Lee, Chang-Wook, Reitz, Rolf D. and Kurtz, Eric. "The Impact of Engine Design Constraints on Diesel Combustion System Size Scaling." *SAE 2010 World Congress Exhibition*. 2010. SAE International. DOI https://doi.org/10.4271/2010-01-0180. URL https://doi.org/10.4271/2010-01-0180.

[9] Tess, Michael J., Lee, Chang-Wook and Reitz, Rolf D. "Diesel Engine Size Scaling at Medium Load without EGR." *SAE International Journal of Engines* Vol. 4 No. 1 (2011): pp. 1993–2009. DOI https://doi.org/10.4271/2011-01-1384. URL https://doi.org/10.4271/2011-01-1384.

[10] Curran, Scott, Onorati, Angelo, Payri, Raul, Agarwal, Avinash Kumar, Arcoumanis, Constantine, Bae, Choongsik, Boulouchos, Konstantinos, Chuahy, Flavio Dal Forno, Gavaises, Manolis, Hampson, Gregory J, Hasse, Christian, Kaul, Brian, Kong, Song-Charng, Kumar, Dhananjay, Novella, Ricardo, Pesyridis, Apostolos, Reitz, Rolf, Vaglieco, Bianca Maria and Wermuth, Nicole. "The future of ship engines: Renewable fuels and enabling technologies for decarbonization." *International Journal of Engine Research* Vol. 25 No. 1 (2024): pp. 85–110. DOI 10.1177/14680874231187954. URL

https://doi.org/10.1177/14680874231187954, URL https://doi.org/10.1177/14680874231187954.

[11] Zhou, Lei, Shao, Aifang, Wei, Haiqiao and Chen, Xi. "Sensitivity Analysis of Heavy Fuel Oil Spray and Combustion under Low-Speed Marine Engine-Like Conditions." *Energies* Vol. 10 No. 8 (2017). DOI 10.3390/en10081223. URL https://www.mdpi.com/1996-1073/10/8/1223.

[12] Zhou, Xinyi, Li, Tie, Wei, Yijie and Wu, Sichen. "Scaling spray combustion processes in marine low-speed diesel engines." *Fuel* Vol. 258 (2019): p. 116133. DOI https://doi.org/10.1016/j.fuel.2019.116133. URL https://www.sciencedirect.com/science/article/pii/S0016236119314875.

[13] Zhou, Xinyi, Li, Tie, Wei, Yijie and Wang, Ning. "Scaling liquid penetration in evaporating sprays for different size diesel engines." *International Journal of Engine Research* Vol. 21 No. 9 (2020): pp. 1662–1677. DOI 10.1177/1468087419889835. URL https://doi.org/10.1177/1468087419889835, URL https://doi.org/10.1177/1468087419889835.

[14] Zhou, Xinyi, Li, Tie, Lai, Zheyuan and Huang, Shuai. "Similarity of split-injected fuel sprays for different size diesel engines." *International Journal of Engine Research* Vol. 22 No. 3 (2021): pp. 1028–1044. DOI 10.1177/1468087419849771. URL https://doi.org/10.1177/1468087419849771, URL https://doi.org/10.1177/1468087419849771.

[15] Zhou, Xinyi, Li, Tie and Yi, Ping. "The similarity ratio effects in design of scaled model experiments for marine diesel engines." *Energy* Vol. 231 (2021): p. 121116. DOI https://doi.org/10.1016/j.energy.2021.121116. URL https://www.sciencedirect.com/science/article/pii/S0360544221013645.

[16] Kaul, Brian, Nafziger, Eric, Kass, Michael, Givens, Willie, Crouthamel, Kevin, Fogarty, John, Satterfield, Andrew, Brabez, Nabila, Brooks, Patrick, Jamieson, Andrew, Williams, Matthew, Blaxill, Hugh and Kristensen, Nikolaj. "Enterprise: a reduced-scale, flexible fuel, single-cylinder crosshead marine diesel research engine." URL https://www.osti.gov/biblio/1528709.

[17] Ranzi, Eliseo, Cuoci, Alberto, Faravelli, Tiziano, Frassoldati, Alessio, Migliavacca, Gabriele, Pierucci, Sauro and Sommariva, Samuele. "Chemical Kinetics of Biomass Pyrolysis." *Energy & Fuels* Vol. 22 No. 6 (2008): pp. 4292–4300. DOI 10.1021/ef800551t. URL https://doi.org/10.1021/ef800551t, URL https://doi.org/10.1021/ef800551t.

[18] RANZI, ELISEO, FRASSOLDATI, ALESSIO, STAGNI, ALESSANDRO, PELUCCHI, MATTEO, CUOCI, ALBERTO and FARAVELLI, TIZIANO. "Reduced Kinetic Schemes of Complex Reaction Systems: Fossil and Biomass-Derived Transportation Fuels." *International Journal of Chemical Kinetics* Vol. 46 No. 9 (2014): pp. 512–542. DOI https://doi.org/10.1002/kin.20867. URL https://onlinelibrary.wiley.com/doi/pdf/10.1002/kin.20867, URL https://onlinelibrary.wiley.com/doi/abs/10.1002/kin.20867.

[19] D.F. Chuahy, Flavio, Finney, Charles E.A., Kaul, Brian C. and Kass, Michael D. "Computational exploration of bio-oil blend effects on large two-stroke marine engines." *Fuel* Vol. 322 (2022): p. 123977. DOI https://doi.org/10.1016/j.fuel.2022.123977. URL https://www.sciencedirect.com/science/article/pii/S0016236122008365.